Axialitic Morphology of Poly(9,9-di-*n*-octyl-2,7-fluorene)

Su-Hua Chen,[†,*] An-Chung Su,[‡,§,*] and Show-An Chen[‡]

Department of Materials Science and Engineering, National Dong Hwa University, Hualien 974, Taiwan, Department of Chemical Engineering, National Tsing Hua University, Hsinchu 300, Taiwan, and Institute of Materials Science & Engineering and Center for Nanoscience & Nanotechnology, National Sun Yat-sen University, Kaohsiung 804, Taiwan

Received August 27, 2006; Revised Manuscript Received October 11, 2006

ABSTRACT: Morphological features of melt crystallized poly(9,9-di-*n*-octyl-2,7-fluorene) (PFO) were examined by means of polarized light microscopy, scanning electron microscopy, and transmission electron microscopy. Upon step-change of temperature from a nematic state at 250 °C to a supercooled melt at $T_c = 140$ or 145 °C, crystallization of PFO proceeds in 3 stages: (1) nucleation to form micrometer-sized leaf-like entities comprising fibrils of slender lamellae, (2) preferred longitudinal fibrillar growth and branching to give axialites, and (3) filling of the "eyes" (formed due to hindered transverse growth) via nucleation of new patches of locally aligned lamellae that are distinctively oriented from the existing axialitic structure. Results of selected-area electron diffraction indicate generally that PFO backbones tend to orient in-plane and perpendicular to the fibrillar axis as a result of preferred growth along the crystallographic *b*-axis. However, with decreasing film thickness, axialitic growth is inhibited; formation of facetted flat-on single crystals (to avoid increasingly unfavorable exposure of lateral surfaces) becomes a more competitive mode of crystallinity development.

Introduction

As one of the "fruit flies" in the study of semiconducting polymers, poly(9,9-di-*n*-octyl-2,7- fluorene) (PFO, chemical structure shown as inset in Figure 3f) has been extensively studied in terms of the phase behavior and the subsequent effects on optoelectronic properties.[1−3] One particularly interesting aspect of PFO is its clear tendency toward development of long-range 3D crystalline order. This renders PFO an ideal vehicle for the elucidation of not only molecular factors affecting molecular packing in conjugated polymers but also to the general crystallization behavior of semirigid chains. Phase transformation and molecular packing in crystalline PFO have been examined by diffraction techniques with assistance from molecular simulation.[4−6] Despite different suggestions on side-chain conformation, it is generally agreed that PFO is nematic above its melting temperature (T_m) of ca. 160 °C, below which PFO crystallizes readily into an orthorhombic structure of large unit cell size ($a = 2.56$ nm, $b = 2.34$ nm, $c = 3.32$ nm, 8 chains), where the slightly noncollinear repeating units are arranged in approximately 2_1-helical fashion with moderate deviations of aromatic rings from coplanarity.[4−6]

At a greater scale, earlier near-field scanning optical microscopic studies by Teetsov and Vanden Bout[7,8] on film morphology of PFO and its close homologues indicated formation of ribbonlike entities after heat treatment at their respective T_m. These ribbons were ca. 20−70 nm wide, in which PFO backbones lay in-plane and transverse to the ribbon axis. Our own electron microscopic observations[5] indicated a broad range of morphological features from strings of nanobeads to flat-on and edge-on lamellar crystals upon melt crystallization of PFO films. Here we extend our earlier studies of melt crystallized PFO single crystals to morphological development in the micrometer scale, i.e., the formation of axialites in PFO films. We show that melt-crystallization of PFO generally results in axialites with the longitudinal axis determined by preferred growth along the crystallographic *b*-axis. The degree of matching between crystallographic orientation and molecular orientation in the nematic melt at the growth front exerts strong effects on the apparent growth rate. With decreasing film thickness, axialitic growth eventually becomes inhibited such that flat-on single crystals may develop. All these observations are explained in terms of the strong preference for PFO crystal growth along the *b*-axis.

Experimental Section

The PFO sample used here was purchased from American Dye Source, Quebec, Canada (Cat. No. ADS129BE). The weight-average molecular mass (M_w) was 65 kDa and polydispersity index PDI) 2.6 as determined via GPC using polystyrene standards. Using a correction factor of 0.37,[9] the true M_w value is estimated to be 24 kDa. Polarized light microscopic (PLM) observations were made by use of a Nikon Eclipse E400-POL microscope equipped with a water-cooled hot stage (Linkman THMS-600, connected to a TMS-91 temperature controller) under protective nitrogen atmosphere. Surface topographic features were examined via secondary electron images (SEI) obtained by use of a field-emission scanning electron microscope (JEOL JSM-6330TF) under an accelerating voltage of 10 kV. Transmission electron microscopic (TEM) studies were performed using a JEOL 3010 instrument under an acceleration voltage of 200 kV at which the combined factor of wavelength and camera length has been carefully calibrated using (111), (200), (220), and (311) reflections from a vapor-deposited Al thin film standard.

Films of submicrometer thickness were drop cast from dilute (ca. 0.3 w/v %) solutions of PFO in toluene on glass substrates. In the case of TEM specimens, a flow-cast procedure by tilting the glass substrate to an upright orientation was adopted; this decreases the film thickness to ca. 100 nm. The as-cast films were then vacuum-dried (in excess of 4 h at ca. 80 °C) before further heat treatments at elevated temperatures. These were routinely started by a brief 1-min treatment at 250 or 210 °C to eliminate previous processing history. This was followed by jumping to a melt crystallization temperature (T_c) of 140 or 145 °C for different

[†] Department of Materials Science and Engineering, National Dong Hwa University.
[‡] Department of Chemical Engineering, National Tsing Hua University.
[§] Institute of Materials Science & Engineering and Center for Nanoscience & Nanotechnology, National Sun Yat-sen University.

10.1021/ma061972f CCC: $33.50 © 2006 American Chemical Society
Published on Web 11/20/2006

durations (from minutes to hours to facilitate observations over different extents of crystallinity development) before subsequent quenching into liquid nitrogen. Note that this translates to a fairly large supercooling (ΔT = ca. 34 or 39 °C) from its equilibrium melting temperature T_m° = 179 °C. All heat treatments were made in the PLM hot stage. For shear-oriented specimens, a manual shearing procedure (i.e., sweeping a blade over the melted thin film) was adopted prior to the heat treatment steps. The PLM specimens, as-cast on the glass substrate, were first examined without a cover slide; these were then sputter-coated with Pt for SEM observations. The TEM specimens were detached from the glass substrate using a dilute HF solution, followed by shadowing (at 60° from plane normal) with a combined Pt/C source prior to TEM examinations.

Results

Axialitic Growth. Given in Figure 1 are morphological features of PFO films after short-term (i.e., 6 min) melt-crystallization at 145 °C and subsequent quenching in liquid nitrogen. From PLM micrographs (Figure 1a,b), elongated (with optically negative birefringence) spherulite-like entities approximately 20 μm in size may be identified from the nematic background. As further revealed by secondary electron images (SEI, Figure 1c,d), these asymmetrically developed "spherulites" turn out to be composed of crystalline "fibrils" (or more precisely, slender edge-on crystalline lamellae) with apparent preference for growth in the axial direction. These are hence more appropriately referred to as *axialites* hereafter. One may note from Figure 1d that the retarded transverse growth is accompanied by protuberance due to gradual tilting and edgewise growth of the sheath lamellae. In the lower left corner of Figure 1e, baby-axialites (ca. 2 μm in size, which apparently nucleated later in time than the well developed axialite at the center of view) may be identified. Under higher magnification (Figure 1f), the leaf-like baby-axialites already exhibit preferred growth along the central podium as well as protuberances of sheath lamellae due to limited degree of branching. Hence these characteristics of axialitic growth may be traced back to the very infant stage. It is then interesting to note that, during this stage of axialitic development, crystalline lamellae are generally oriented with the *c*-axis lying in-plane (and transverse to the "fibrillar" axis) where the *a*-axis along the film normal. This is demonstrated by a representative bright-field image (Figure 1g) and the corresponding selected area electron diffraction pattern (Figure 1h, taken from the encircled central region in Figure 1g).

Effects of Shear Orientation. To elucidate further the preference for in-plane backbone orientation with *a*-axis pointing toward film normal in PFO axialites, shear-oriented specimens were examined. As shown in Figure 2a,b, these shear oriented specimens are characterized by a background of extended nematic domains (each about 10 μm in width) running along the shear direction. As judged from the birefringence color, backbone axes are not exactly aligned in the shear direction but are alternatively tilted from the shear direction in neighboring domains. It is then interesting to note that the long axes of axialites formed in these specimens are generally aligned to the backbone orientation within each nematic domains. This results in encouraged growth in quadrants where the backbone orientation in the nematic state coincides with the crystalline *c*-axis as well as retarded development of the opposite quadrants, as more clearly demonstrated in the blown-up view (Figure 2c). Corresponding SEI (Figure 2d) shows that the better-developed quadrants are characteristically lower in surface ruggedness as compared to the retarded quadrants. For these densely arrayed axialites, topographic features of protuberances from sheaf lamellae are further enhanced due to differences in orientation of sheath lamellae from neighboring axialites. Note also the presence of micrometer-sized baby-axialites in the upper right corner: these are also aligned parallel to the mature axialites and with more rugged lower quadrants.

Space-Filling of Crystallites. Figure 3 shows morphological features after prolonged melt crystallization. The PLM micrographs (Figure 3a,b) demonstrate large (ca. 60−80 μm in diameter) but blurred spherulite-like features with generally negative birefringence. Under high-magnification SEM (Figure 3c), one observes that these spherulite-like entities essentially comprise locally aligned fibrils that appear either as branches developed from the initial axialitic structure or as disoriented patches. The latter are particularly abundant in (but not limited to) the "eye" regions of the basic axialitic structure. This implies that, during the extended period of melt crystallization, new axialites are nucleated but confined to interstitial space or in the "eyes" of existing axialites. At this stage, the clear preference for *a*-axis to align in the film normal direction in the early stage of crystallization can no more be identified: various orientations are now observed, as demonstrated in Figure 3d−g. Nevertheless, the general trend for backbones (or the crystallographic *c*-axis) to lie in-plane persists even to this later stage of crystallization.

Effects of Decreasing Film Thickness. Given in Figure 4 are particular observations around a bubble (dewetted during film casting), which serve as convenient demonstrations of film thickness effects. In Figure 4a,b, the PFO matrix exhibits characteristic space-filled axialites (more clearly identifiable with gypsum plate inserted). As film thickness decreases toward the matrix-bubble boundary, nucleation density (per plan-view area) decreases, leaving coarse treelike axialitic texture (Figure 4c,d). In the interstitial region between the "tree-branches," flat-on single crystals are allowed to develop (Figure 4e,f) in the absence of competition from axialitic nucleation. As we have shown previously, these flat-on single crystals of PFO give clear (00*l*) zone pattern, i.e., PFO backbones (and the crystallographic *c*-axis) lie along film normal. In addition, these single crystals are slender, sword-like in shape with clear faceting of {100} and {110} planes, in agreement with previous TEM observations on PFO single crystals.[5] In other words, growth along the crystallographic *b*-axis is preferred, consistent with the asymmetric growth habit in the axialites. Figure 4g shows the magnified view of a single crystal of incomplete faceting. Note the grainy features in the scale of ca. 10 nm.

Discussion

Preferred Growth along the Crystallographic *b*-Axis. From our observations above, it may be concluded that one of the key characteristics in the melt crystallization of PFO is the preferred growth (whether in single crystals or in axialites) along the crystallographic *b*-axis. Origin of this growth habit is not yet clear but the previously proposed model[5] of molecular packing may provide some hints. In the model, PFO backbone are stretched along the *c*-axis whereas alkyl side chains are fully extended transverse to the backbone; each pair of the alkyl side chains from a given monomer unit embraces a neighboring PFO backbone. It turns out that this paired embracement propagates along the *a*-axis: assuming this embracing is kinetically slow to achieve, preferred growth along the *b*-axis would be a natural consequence.

Preferred Crystal Orientation. On the premise of preferred growth along *b*-axis, two possible crystal orientations bear advantage in the competition for crystal growth in films. In one

CDV

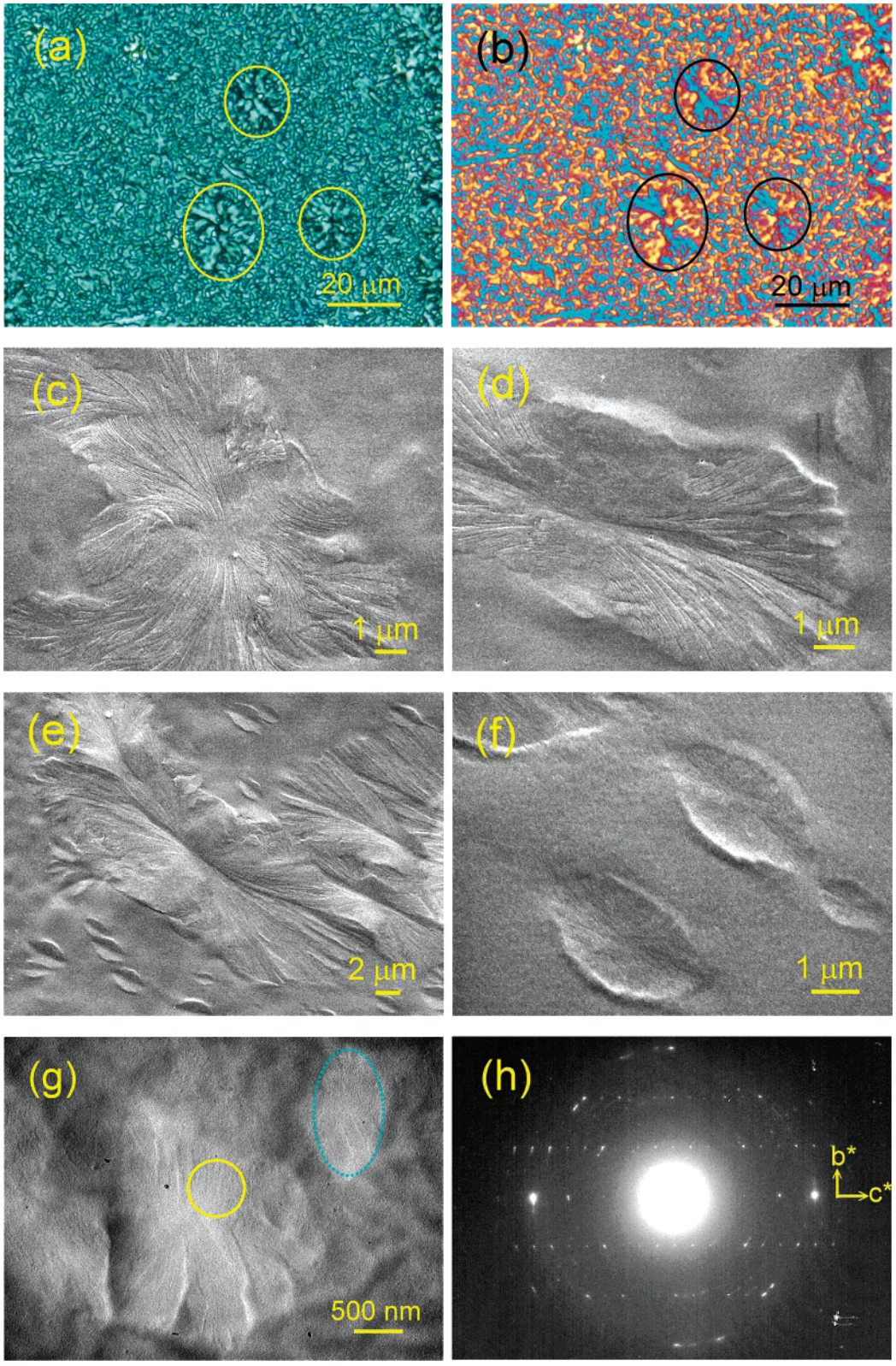

Figure 1. Axialitic morphology of PFO films melt-crystallized for 6 min at 145 °C, followed by quenching in liquid nitrogen: (a,b) PLM micrographs without or with gypsum plate inserted, (c−f) SEI at several locations under different magnifications, and (g) a representative BFI and (h) the corresponding SAED pattern. The axialites first appear as leaf-like entities (f), which grow and splay mainly in the axial direction (d) and become less anisotropic with transversely nucleated branches (c). A representative BFI image (g) and the corresponding SAED pattern (h, taken from the axialite at the central view, slightly rotated to align *b**-axis with the meridian) indicate that molecular chains run transverse to the long axis of fibrillar features that correspond to slender edge-on crystalline lamellae. Note the presence of a junior-axialite in the upper right corner of part g.

case, the backbones (and the *c*-axis) lie in-plane: with preferred in-plane crystal growth along the *b*-axis, the *a*-axis is automatically oriented toward film normal. This agrees with what we have basically observed in the axialitic development. The other possibility is that the backbones lie along film normal, this agrees with the single crystal case. Deviations from these two configurations will result in limited space for crystal development in these relatively thin films. The observed transition in

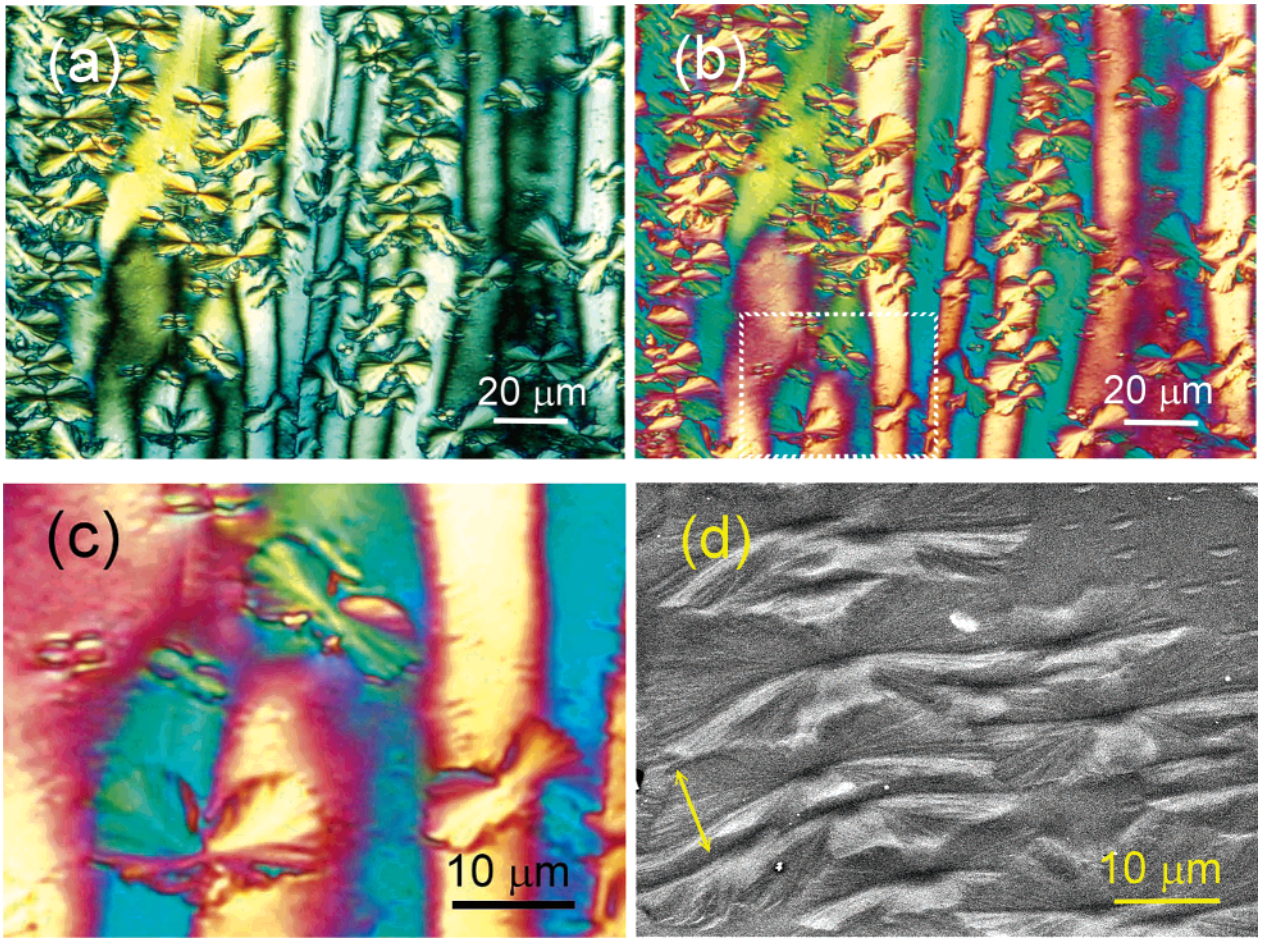

Figure 2. Enhanced nucleation in oriented PFO films manually sheared at 250 °C, melt crystallized at 140 °C for 6 min, followed by quenching in liquid nitrogen: A high density of axialites with their long axes lying perpendicular to the shear direction are easily identified in PLM micrographs (a) without or (b) with gypsum plated inserted. In the background are slender arrays of nematic domains running along the N−S direction of shear action. Details of the asymmetric quadrant development are shown by a blown-up view (c) and SEI (d, shear direction indicated by the two-way arrow), giving finer features of encouraged vs hindered quadrant development due to chain orientation in the nematic domains. Note the micrometer-sized baby-axialites in the upper right corner of part d; these are also aligned parallel to the adult-axialites in the central view.

morphological preference from axialites to single crystals with decreasing film thickness, however, remains to be explained. We offer our explanations below, emphasizing effects from preferred growth and geometrically confined development of PFO crystals in these moderately thin films.

Preparation of polymer single crystals from thin films in the melt state is in fact a well adopted practice for preparation of TEM specimens for crystallographic analysis.[10−12] Traditional wisdom dictates that formation of single crystals in the 3D melt state is difficult as elastic force from entangled network results in resistance to the reeling-in of crystallizing chains from the melt pool to the growth front;[13,14] competing processes from (primary or secondary) nucleation may then prevail, resulting in polycrystalline aggregates such as spherulites. However, with preferred growth along the *b*-axis, axialites of PFO in thin films would correspond to very limited *a*-dimension and hence be subjected to large penalty (per volume basis) from the exposed *b*−*c* surfaces. This explains the inhibited growth of PFO axialites toward the periphery of bubble: formation of micrometer-sized single crystals that, if developed flat-on, are much lower in free energy penalty from lateral surfaces and hence thermodynamically preferred.

It follows that orientation of nuclei should bear little relevance in the early stage of axialitic development: it is growth rate that determines the crystal orientation. Nuclei oriented improperly (that is, with the *a*-axis deviating significantly from film normal) have limited space for growth along the *b*-axis and hence are less competitive in reaching discernible size. This also explains the minor appearance of off-orientation patches of axialites in interstitial regions where "properly oriented" lamellae failed to fill the space after prolonged melt crystallization. Note that a similar observation of growth rate-determined crystal orientation has been reported[15] in the case of confined-space crystallization in amorphous−crystalline diblock copolymers of layered morphology.

Increased Nucleation Density in Sheared Specimens. Some comments are in order on the apparent increase of nucleation density in sheared specimens (Figure 2b vs Figure 1b). This may include contributions from not only shear-enhanced nucleation as one would generally expect but also the highly selective growth along the *b*-axis on the basis of the following arguments. As we have noted earlier, within the present range of film thickness, mechanical shear resulted in slender arrays of alternatively tilted (from the shear direction) nematic domains that are ca. 10 μm in width. Axialitic growth of a quadrant is encouraged if backbone orientation of the nematic matches that in this particular quadrant and vice versa (Figure 2c). The preferred growth within a particular nematic domain eventually leads to the growth front to reach a neighboring domain, which retards axialitic growth as molecular orientation therein deviates significantly from the preferred crystal growth direction. Hence, alternative orientations in arrays of nematic domains eventually

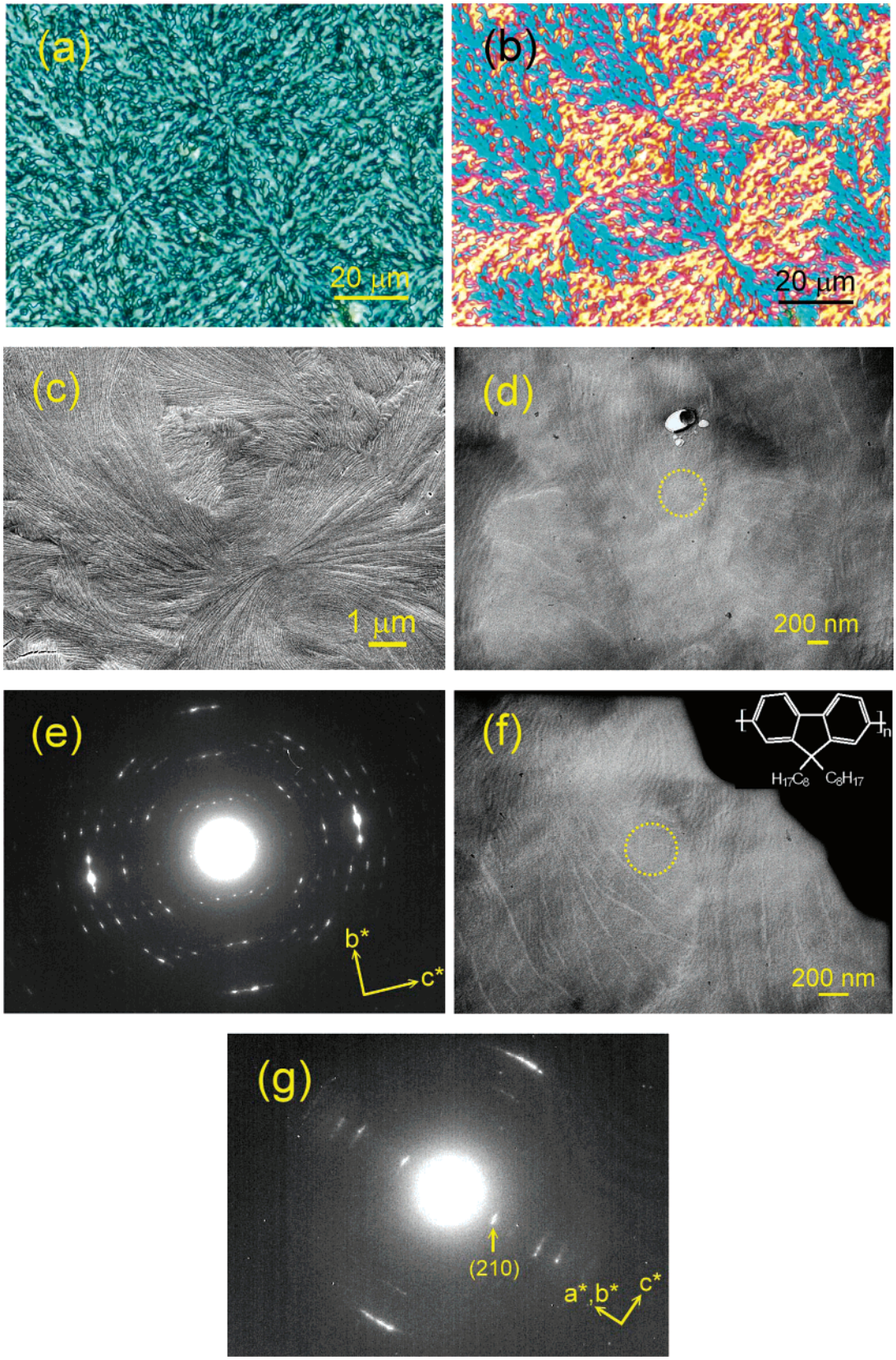

Figure 3. PLM micrographs (a) without or (b) with gypsum plated inserted, showing space-filled axialites in PFO films melt crystallized for 1 h at 145 °C, followed by quenching in liquid nitrogen. SEI in part c shows that space-filling is achieved by fibrils nucleated and grew within the "eye" regions in the later stage of melt crystallization. These space-filling fibrils run nearly perpendicular to the axialitic fibrils. Representative BFIs (d,f) and corresponding SAEDs (e,g) indicate preference persists for *c*-axis to lie in-plane, but different orientations of *a*- and *b*-axes are now identifiable.

serve to constrain axialitic development to ca. 20 μm (within the present range of observation time), as may be observed in Figure 2b. The temporarily halted growth of existing axialites allows for the nucleation and (similarly constrained) growth of younger axialites, which would contribute at least partly to the apparently increased plan-view density of axialites.

CDV

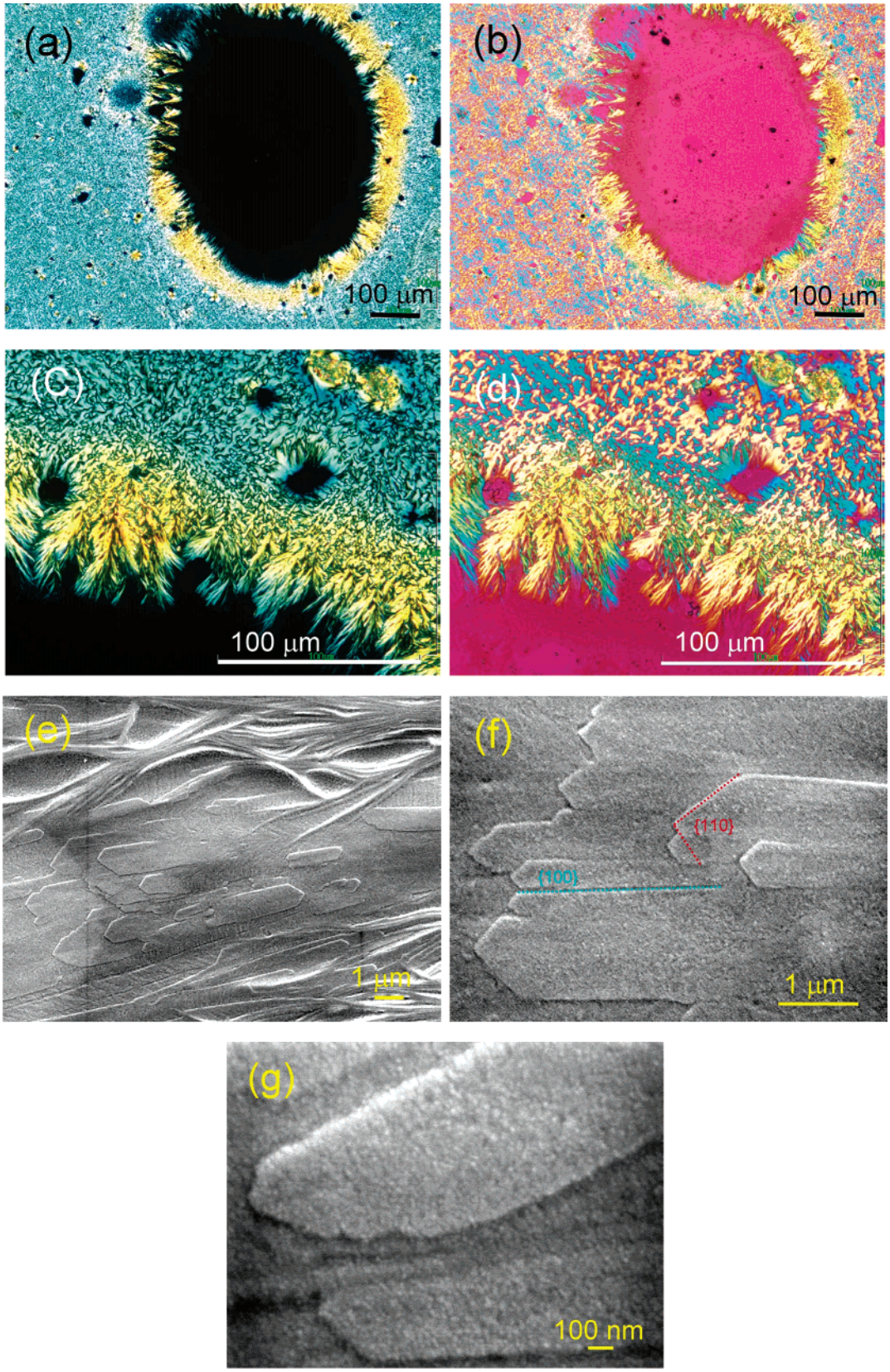

Figure 4. With decreasing film thickness, flat-on single crystals tend to develop. This is shown by PLM micrographs (a−d) and SEI (e−g) near the edge of a dewetted pore in a PFO film melt crystallized at 145 °C for 14 h, followed by quenching in liquid nitrogen. Instead of fine axialitic texture in the bulk matrix, there are coarse treelike features around bubble periphery as a result of decreased nucleation density (per plan-view area) of space-filling axialitic patches. In regions between "tree-branches," single crystals with {100} and {110} facets develop upon prolonged melt crystallization (e,f). Note the grainy features of these single crystals under high magnification (g).

General Comments on Morphology of Conjugated Polymers. In view of the backbone rigidity, conjugated polymers are believed to crystallize in a manner quite different from traditional polymers of flexible backbones. Intuitively, the fringed-micelle picture appears appropriate and the crystals are likely to be limited in size; this is indeed born out in early

morphological studies of conjugated polymers where structural investigation has therefore been focused to the molecular level within a unit cell.[16] Nevertheless, recent observations on regioregular poly(3-*n*-alkyl-2,5- thiophene)s[17,18] and poly(2,5-di-*n*-alkyl-1,4-phenylenevinylene)s[19,20] indicated formation of rod- or stringlike entities in nanometer scale, in which the conjugated backbones lie in-plane and orthogonal to the long axis. The present case of PFO serves as a first example for further morphological development at a greater length scale that extends the hierarchy of supramolecular aggregation to the next level. The basic mechanism behind this high-level molecular aggregation remains unclear; it is apparent that there are more to add to the conventional fringed-micelle picture to allow for supramolecular aggregation at this length scale. One possible model could be the coalescence of nanoscaled crystallites,[21,22] which calls for a modified view that each nanograin must be able to attach and rotate through thermal activation to achieve concerted orientation with its immediate neighbors. This is beyond the scope here and will be addressed in a future occasion.

Conclusion

Morphological features in melt crystallized PFO films are presented. These may be generally categorized as axialitic, with preferred orientation of crystallographic *b*- and *c*-axes lying in-plane. With decreasing film thickness, axialitic growth becomes inhibited, allowing the formation of flat-on single crystals. All these observations may be explained in terms of the strong preference for PFO crystal growth along the *b*-axis. Consistent with this picture of growth dominance, backbone orientation in the nematic melt is observed to exert clear anisotropic effects on axialitic development.

Acknowledgment. Financial support from the National Science Council under Contract Nos. NSC95-2221-E-007-267 and NSC95-2752-E-007-007-PAE are gratefully acknowledged.

References and Notes

(1) Kraft, A.; Grimsdale, A. C.; Holmes, A. B. *Angew. Chem., Int. Ed.* **1998**, *37*, 402.
(2) Neher, D. *Macromol. Rapid Commun.* **2001**, *22*, 1365.
(3) Scherf, U.; List, E. J. W. *Adv. Mater.* **2002**, *14*, 477.
(4) Grell, M.; Bradley, D. D. C.; Ungar, G.; Hill, J.; Whitehead, K. S. *Macromolecules* **1999**, *32*, 5810.
(5) Chen, S. H.; Chou, H. L.; Su, A. C.; Chen, S. A. *Macromolecules* **2004**, *37*, 6833.
(6) Chunwaschirasiri, W.; Tanto, B.; Huber, D. L.; Winokur, M. J. *Phys. Rev. Lett.* **2005**, *94*, 107402.
(7) Teetsov, J. A.; Vanden Bout, D. A. *J. Am. Chem. Soc.* **2001**, *123*, 3605.
(8) Teetsov, J.; Vanden Bout, D. A. *Langmuir* **2002**, *18*, 897.
(9) Grell, M.; Bradley, D. D. C.; Long; X.; Chamberlain, T.; Inbasekaran, M.; Woo, E. P.; Soliman, M. *Acta Polym.* **1998**, *49*, 439.
(10) Lotz, B.; Lovinger, A. J.; Cais, R. E. *Macromolecules* **1988**, *21*, 2375.
(11) Bu, Z.; Yoon, Y.; Ho, R. M.; Zhou, W.; Jangchud, I.; Ebby, R. K.; Cheng, S. Z. D.; Hsieh, E. T.; Johnson, T. W.; Geerts, R. G.; Palackal, S. J.; Hawley, G. R.; Welch, M. B. *Macromolecules* **1996**, *29*, 6575.
(12) Ho, R. M.; Lin, C. P.; Hsieh, P. Y.; Chung, T. M.; Tsai, H. Y. *Macromolecules* **2001**, *34*, 6727.
(13) Wunderlich, B. *Macromolecular Physics*; Academic: New York, 1976; Vol. 2.
(14) Rieger, J.; Mansfield, M. L. *Macromolecules* **1989**, *23*, 8310.
(15) Zhu, L.; Calhoun, B. H.; Ge, Q.; Quirk, R. P.; Cheng, S. Z. D.; Thomas, E. L.; Hsiao, B. S.; Yeh, F.; Liu, L.; Lotz, B. *Macromolecules* **2001**, *34*, 1244.
(16) For a recent review, see: Winoukur, M. J.; Chunwachirasiri, W. *J. Polym. Sci., Polym. Phys.* **2003**, *41*, 2630.
(17) Kim, D. H.; Park, Y. D.; Jang, Y.; Yang, H.; Kim, Y. H.; Han, J. I.; Moon, D. G.; Park, S.; Chang, T.; Chang, C.; Joo, M.; Ryu, C. Y.; Cho, K. *Adv. Funct. Mater.* **2005**, *15*, 77.
(18) Kline, R. J.; McGehee, M. D.; Kadnikova, E. N.; Liu, J.; Fréchet, J. M. J.; Toney, M. F. *Macromolecules* **2005**, *38*, 3312.
(19) Chen, S. H.; A. C. Su, A. C.; Han, S. R.; Chen, S. A.; Lee, Y. Z. *Macromolecules* **2004**, *37*, 181.
(20) Chen, S. H.; Su, C. H.; Su, A. C.; Chen, S. A. *J. Phys. Chem. B* **2004**, *108*, 8855.
(21) Métois, J. J.; Gauch, M.; Masson, A.; Kern, R. *Surf. Sci.* **1972**, *30*, 43.
(22) Shen, P.; Fahn, Y. Y.; Su, A. C. *Nano Lett.* **2001**, *1*, 299.

MA061972F